Neville, R. M., Monti, A., Hazra, K., Scarpa, F., Remillat, C., & Farrow, I. R. (2014). Transverse stiffness and strength of Kirigami zero- PEEK honeycombs. Composite structures, 114, 30-40. 10.1016/j.compstruct.2014.04.001

Elsevier Editorial System(tm) for Composite Structures
Manuscript Draft

Manuscript Number:

Title: Transverse stiffness and strength of Kirigami zero-ν PEEK honeycombs

Article Type: Full Length Article

Keywords: Polymers; Honeycomb; Buckling; Analytical modelling; Mechanical testing; Forming

Corresponding Author: Mr. Robin M Neville, MEng

Corresponding Author's Institution: University of Bristol

First Author: Robin M Neville, MEng

Order of Authors: Robin M Neville, MEng; Arthur Monti; Kalyan Hazra; Fabrizio Scarpa; Chrystel Remillat; Ian R Farrow

Abstract: This work describes the manufacture and characterisation of a PEEK-based zero Poisson's ratio honeycomb (SILICOMB) produced using Kirigami-inspired cutting and folding techniques. The flatwise compression and transverse shear properties of the structure are determined through ASTM mechanical testing, and the results compared against commercially available honeycombs, including several other zero Poisson's ratio cellular structures. An analytical model to predict the shear strength is compared to the results. SILICOMB specimens are found to have lower stiffness compared to other honeycomb configurations, but comparable strength. Factors influencing the results and variations to the manufacturing process are discussed.

Suggested Reviewers: Joseph Grima
Professor, Chemistry, University of Malta
joseph.grima@um.edu.mt
Zero Poisson's ratio materials

Farhan Gandhi
Professor, Aeronautical, Rensselaer Polytechnic
gandhf@rpi.edu
ZPR honeycombs, characterisation

Dan Zenkert
Professor, Aeronautical and Vehicle Engineering, KTH
danz@kth.se
Sandwich structures and honeycombs

Andrew Alderson
Principal Research Fellow, Materials and Engineering Research Institute, Sheffield Hallam University
a.alderson@shu.ac.uk
Auxetic composites

Fabrizio Scarpa, Laurea, PhD, FRAeS
Professor of Smart Materials and Structures
Advanced Composites Centre for Innovation and Science
Aerospace Engineering
University of Bristol
Queen's Building
University Walk, Bristol, BS8 1TR
United Kingdom
Tel: +44 (0)117 33 15306

Monday, 27 January 2014

Editorial Board
Composite Structures

Subject: Submission to Composite Structures

Please find included copy of the manuscript: "Transverse stiffness and strength of Kirigami zero-ν PEEK honeycombs" by Neville, Monti, Hazra, Scarpa, Remillat and Farrow.

The paper describes an experimental and modeling characterisation of novel PEEK honeycombs with zero Poisson's ratio manufactured with Kirigami techniques. The mechanical performance of these honeycombs is also benchmarked against commercial cores.

Please note that the Contact Author for this submission is **Mr Robin Neville**.

Do contact us for further queries if needed. We will be happy to answer back.

Regards,

Prof Fabrizio Scarpa
ACCIS

Transverse stiffness and strength of Kirigami zero-ν PEEK honeycombs

R. M. Neville*, A. Monti, K. Hazra, F. Scarpa, C. Remillat, I. R. Farrow

Advanced Composites Centre for Innovation and Science (ACCIS), University of Bristol, BS8 1TR Bristol, UK

** Tel: 0044 (0) 117 3315 777*

** Email: rn7318@bristol.ac.uk*

Abstract

This work describes the manufacture and characterisation of a PEEK-based zero Poisson's ratio honeycomb (SILICOMB) produced using Kirigami-inspired cutting and folding techniques. The flatwise compression and transverse shear properties of the structure are determined through ASTM mechanical testing, and the results compared against commercially available honeycombs, including several other zero Poisson's ratio cellular structures. An analytical model to predict the shear strength is compared to the results. SILICOMB specimens are found to have lower stiffness compared to other honeycomb configurations, but comparable strength. Factors influencing the results and variations to the manufacturing process are discussed.

Keywords: Polymers; Honeycomb; Buckling; Analytical modelling; Mechanical testing; Forming.

1 Introduction

The mechanical properties of cellular materials are largely dependent on the configuration of their cell walls and the core material itself [1]. The Poisson's ratio of honeycomb configurations can vary from 1 (regular hexagonal honeycomb), to large positive and negative values in centresymmetric configurations [2]–[5]. Non-centresymmetric topologies (hexachiral and tetrachiral) exhibit Poisson's ratios around -1 [6]–[8]. Structures exhibiting negative Poisson's ratio (NPR) are also known as auxetic [9]. An interesting case is represented by structures with zero Poisson's ratio (ZPR), which have no coupling between orthogonal in-plane deformations. The ZPR behaviour implies therefore that a uniaxial tensile loading does not result in any lateral mechanical response. Similarly, when the structure is subjected to bending no synclastic or anticlastic curvature is observed; the structure assumes a cylindrical shape [10]. Evans [11] reports how auxetic honeycombs facilitate the manufacturing of doubly-curved sandwich structures compared to honeycombs with positive Poisson's ratio, because they do not generate anticlastic curvature which must be suppressed. For the same reasons, zero-ν honeycombs are more suitable for cylindrical sandwich structures than either auxetic or conventional honeycombs [10]. Honeycombs with near-zero Poisson's ratio (FlexCore) are also available commercially, and are specifically designed for improved formability [12]. Existing work has also focused on using zero-ν honeycombs for 1D spanwise morphing of wings [13] and biomedical scaffolds [14]. Zero Poisson's ratio configurations have been created in different ways. Hexagonal cores can be elongated until the cells are rectangular; this so-called "ox-core" has a Poisson's ratio of approximately zero [15]. HexCel FlexCore achieves near-zero ν through corrugated cell walls [12]. Grima and co-workers proposed a honeycomb comprised of semi-re-entrant "chevron"-shaped cells [10], [16]. Olympio and Gandhi proposed a honeycomb with a mixture of re-entrant and non-re-entrant cells (accordion honeycomb) [13], [17]. The "chevron" and "accordion" honeycombs both achieve zero ν through a balance of re-entrant (auxetic) and non-re-entrant features. The SILICOMB geometry achieves ZPR through a geometry which is inspired by the tessellation of β-cristobalite lattice [18], [19]. In previous works some of the authors investigated the Poisson's ratio and transverse shear modulus of SILICOMB through finite element analysis and mechanical testing of 3D printed samples [20]. SILICOMB configurations have been also used to produce curved cellular structures exhibiting shape morphing [21] and large energy absorption when passing through a negative stiffness regime [22]. In this paper the SILICOMB geometry was produced from PEEK film using a Kirigami cutting and folding technique. The Kirigami process essentially involves cutting and folding flat sheets of material to form 3D cellular structures [23]. A feature of the process is the considerable

control over the geometry of the structure; by changing the pattern of cuts and folds on the 2D material, the cell shape and gauge thickness of the resulting 3D cellular structure can be controlled locally and globally. This allows the user to build complex honeycomb geometries with built-in features to suit a specific purpose; from one-step integral honeycomb panels and wingbox configurations [23]–[26], to complex graded honeycomb topologies with mixed conventional-auxetic behaviour [27].

The paper describes the manufacturing, testing and modelling of the transverse compressive and shear stiffness and strength of Kirigami-based SILICOMB honeycombs made with poly(ether-ether-ketone) Victrex Aptiv PEEK film. PEEK is a linear, aromatic and semi-crystalline thermoplastics, with very high melting temperature, and good combination of mechanical strength, dielectric and thermal capacity, and complex shape forming. It is currently evaluated and used in high-end aerospace structural applications, from the A400 M cargo floor [28] to spacecraft constructions [29]. Ventilation holes were included in the honeycomb design to let escape trapped air in the cells at high temperatures for possible spacecraft applications. Current manufacturing processes used in sandwich constructions for spacecraft applications involve the drilling of venting holes as a post-processing of the production of the whole sandwich panel, with significant labour costs involved [15]. The Kirigami process allows cutting of the holes on the flat sheet of PEEK before folding, making the whole process interesting from an industrial perspective. ASTM-type flatwise compression and single-lap transverse shear tests have been carried out on the PEEK Kirigami SILICOMB specimens, and the results are compared to commercially available honeycombs. Moreover, analytical and Finite Element models describing the compressive and shear strength of the honeycombs have been developed to understand the dependence of these quantities on the geometry parameters of the unit cells. To the best of the Authors' knowledge, this is the first time that a Kirigami-based PEEK honeycomb has been designed and characterised from a mechanical point of view. Moreover, no other ZPR PEEK-based honeycomb in flat panel configuration has been investigated before.

2 Manufacturing and testing

2.1 Kirigami process

The SILICOMB geometry (see Figure 1) can be composed by interlocking two sets of slotted zigzagging strips (see Figure 2). Using this geometry breakdown allows the use of one set of modular moulds throughout the manufacturing process used. Slotted strips have been cut from PEEK Aptiv film using a Blackman & White Genesis cutter (see Figure 3a). The aforementioned ventilation holes are 0.25mm in diameter. A purpose-built tool (see Figure 3b) was used to form the slotted strips into the desired 'zigzag' geometry using

a Formech FM1 vacuum forming table. Prior to forming, tape was used to fix the strips to the tool as closely as possible to minimise the mobility of the strips during the forming process (see Figure 3c). Vacuum and heat were applied. The temperature was monitored using a thermocouple attached directly to the tool face. Upon reaching 150°C the heaters were turned off and the strips were allowed to cool gradually while still under vacuum. The 150°C temperature was selected as a cut-off point because it is sufficiently above PEEK's glass transition temperature of 143°C [30] to allow for any thermocouple error. Due to the residual heat in the heaters and tooling, the film has been put to rest at around 150°C for several minutes after switching off the heaters. This processing window is very short, however the film needs less than a minute above its Tg to achieve permanent shape change [30]. Figure 3d shows the strips after forming. The strips were then slotted together to produce the SILICOMB geometry (see Figure 2, Figure 3e). Once the samples were assembled and had been cleaned using acetone, 3M Scotch-Weld Epoxy adhesive was mixed and applied to the joints using the provided spatula (see Figure 3f). The specimens were cured for 1 hour at 70°C in an oven. Weights were placed on the samples to keep them flat during cure (see Figure 3g).

2.2 Testing

Samples were created for compression and shear tests according to relevant ASTM standards [31], [32]. Table 1 shows details of all specimen types. Specimen geometry was defined in terms of rows and columns. Rows and columns are repetitions of the unit cell (see Figure 1) along the 1 and 2-directions, respectively. For all the tests self-aligning plates were used (Figure 4). During the flatwise compression tests a Roell-Amsler machine with 25kN load cell was used. The shear tests were performed using an Instron tensile machine with 100kN load cell. Tests were displacement controlled, with the displacement rate set to 0.5mm/minute to produce failure in 3-6 minutes, as specified in the standards [31], [32].

3 Analytical modelling

An analytical model was created to predict the buckling strengths of the SILICOMB geometry following a procedure similar to the analysis applied to hexagonal honeycombs by Gibson and Ashby [1] and Zhang and Ashby [33]. The model assumes that the buckling load of a unit cell is the sum of the buckling loads of critical cell walls, with the choice of which walls to consider critical depending upon the type of loading. Figure 5 shows how the SILICOMB unit cell can be considered as a group of 8 walls with width l and 8 walls with width $h/2$. The buckling coefficients for both types of wall under different loadings and boundary conditions (BCs) are shown in Table 2. Using this information we construct a unit cell model for each loading condition.

3.1 Compression

Considering the cell walls as plates in compression one can use the critical buckling load formula [34]:

$$P_{cr} = \frac{KEt^3}{b(1-\nu^2)} \quad (1)$$

Substituting in the relevant values from Table 2 the critical buckling load for each type of wall becomes:

$$P_{cr,l} = \frac{K_l E t^3}{l(1-\nu^2)} \quad (2)$$

$$P_{cr,h} = \frac{2K_h E t^3}{h(1-\nu^2)} \quad (3)$$

Zhang and Ashby assume in their compression analysis of double-walled honeycombs [33] that all the walls buckle simultaneously because they are forced to undergo the same deflection, despite the fact that the double wall has a significantly higher buckling load. This approach gives good results when compared against experimental data, and it is reasonable to assume the same behaviour for SILICOMB despite the difference between $P_{cr,l}$ and $P_{cr,h}$. For equilibrium along the 3-direction one can equate the cell wall buckling loads to the external compressive stress computed as the ratio between the sum of the cell wall buckling loads and the unit cell area:

$$\sigma_{3\,cr} = \frac{8P_{cr,l} + 8P_{cr,h}}{8hl\cos\theta\cos\phi} \quad (4)$$

Substituting in (2) and (3) gives:

$$\sigma_{3\,cr} = \frac{E\beta^3\left(K_l + 2\frac{K_h}{\alpha}\right)}{\alpha(1-\nu^2)\cos\theta\cos\phi} \quad (5)$$

Where $\alpha = h/l$ and $\beta = t/l$. Substituting in values from Table 1 and Table 2 one can find $\sigma_{3\,cr}$ for all sides simply supported (SS), and for ends simply supported, edges clamped (SS/C):

$$\sigma_{3_{cr}}^{SS} = 0.49\ MPa \quad (6)$$

$$\sigma_{3_{cr}}^{SS/C} = 0.97\ MPa \quad (7)$$

3.2 Shear

Considering the cell walls as plates undergoing shear loading, it is possible to use the following formula for the critical load [34]:

$$Q_{cr} = \frac{CEt^3}{b(1-\nu^2)} \quad (8)$$

Substituting in the relevant values from Table 2, the critical buckling load for each type of wall is:

$$Q_{cr,l} = \frac{C_l E t^3}{l(1-\nu^2)} \quad (9)$$

$$Q_{cr,h} = \frac{2C_h E t^3}{h(1-\nu^2)} \quad (10)$$

In the case of shear loading the selection of the critical walls becomes less evident. It is no longer appropriate to consider the walls to be contributing equally to the resistance to the external load, because the way in which the cell walls react to the external loading depends on their orientation relative to the load. As in [1], it is possible assume that the most highly loaded (critical) wall will buckle first, with the rest of the structure following suit due to the change in boundary conditions caused by the buckled wall. A finite element model of the SILICOMB unit cell was therefore used to determine which walls are critical. MSC PATRAN and NASTRAN finite element software was used to create the models. CQUAD4 2D shell elements were used throughout the model with an element size of 2.5mm; this mesh density sufficiently captures the stress gradients in the walls. The degrees of freedom of each free edge of the unit cell were coupled to those of its

counterpart on the opposite side of the unit cell using multi-point constraints (MPCs); thus mimicking a continuous honeycomb. The bottom face was fully clamped. On the top face all rotations and 3-direction translation were restrained. An MPC was used to preserve the shape of the top face while allowing motion in the 1 and 2 directions. This analysis was repeated for a range of values of α, to ascertain how sensitive the shear stress distribution is to variations in the geometry. Plots of Von Mises stress are shown in Figure 6. It can be seen that there is no change in critical walls across quite large perturbations in α.

13-direction

Figure 6 shows that for 13-direction shear the *l*-walls are critical. Considering equilibrium along the 1-direction the critical shear stress can be determined by averaging the buckling loads of the *l*-walls over the unit cell area:

$$\tau_{13_{cr}} = \frac{8Q_{cr,l}\cos\theta}{8hl\cos\theta\cos\phi} = \frac{Q_{cr,l}}{hl\cos\phi} \quad \textbf{(11)}$$

Substituting in (9) gives:

$$\tau_{13_{cr}} = \frac{C_l E\beta^3}{\alpha(1-\nu^2)\cos\phi} \quad \textbf{(12)}$$

As previously shown, the equation can be evaluated for different boundary conditions; all walls simply supported (SS) and all walls clamped (C):

$$\tau_{13_{cr}}^{SS} = 0.27\ MPa \quad \textbf{(13)}$$

$$\tau_{13_{cr}}^{C} = 0.51\ MPa \quad \textbf{(14)}$$

23-direction

Figure 6 shows that for 23-direction shear the inner *h*-walls are critical. Considering the equilibrium along the 2-direction and the contribution to the shear resistance given only by those particular walls one obtains:

$$\tau_{23_{cr}} = \frac{4Q_{cr,h}\cos\phi}{8hl\cos\theta\cos\phi} = \frac{Q_{cr,h}}{2hl\cos\theta} \quad (15)$$

Substituting in (10) gives:

$$\tau_{23_{cr}} = \frac{C_h E\beta^3}{\alpha^2(1-\nu^2)\cos\theta} \quad (16)$$

When all the walls are considered simply supported (SS) or clamped (C), the critical shear stresses for the SILICOMB cellular structures manufactured assume the following values:

$$\tau_{23_{cr}}^{SS} = 0.23\ MPa \quad (17)$$

$$\tau_{23_{cr}}^{C} = 0.39\ MPa \quad (18)$$

4 Results and discussions

Figure 7, Figure 8 and Figure 9 show the comparison between the experimental stress-strain curves and the analytical strength predictions. In the case of flatwise compression, the stiffnesses are all very similar, and the specimens fail at a similar load and strain by global buckling, resulting in a smooth peak. From Figure 7 it can be seen that the experimental results for the compression fall between the analytical SS and C predictions, suggesting that the real boundary conditions are somewhere between clamped and simply supported, as already indicated in [33]. Figure 8 and Figure 9 show the shear stress-strain curves for the sample categories A and B respectively. In this case some perturbations to the stiffness curves in the linear region can be observed, suggesting that some small failures occurred prior to global collapse, possibly the onset of local buckling. The specimens failed also in this case by global buckling, and for the 13-direction shear case this was followed by the formation of cracks at the ventilation holes, as shown in Figure 10

To make an effective comparison between honeycombs made from different materials and relative densities, it is necessary to normalise the properties of the cellular solids in such a way as to take these differences into account. In this work, the following identities have been used to normalise honeycomb properties for flatwise compression:

$$\frac{property/E_0}{\rho^*/\rho_0} \quad \textbf{(19)}$$

And in the case of shear:

$$\frac{property/G_0}{\rho^*/\rho_0} \quad \textbf{(20)}$$

Terms with a superscript * are related to the honeycomb, and terms with a subscript 0 are related to the constituent material. Material property values used in the normalisation, and the sources thereof, are shown in

Table 3. There is some disagreement in open literature about the mechanical properties of Nomex paper. The DuPont datasheet [35] focuses on other physical properties, and does not provide stiffness values. Zhang and Ashby [33] report a relatively low elastic modulus of 0.9 GPa, and assume isotropy with ν = 0.4 to calculate the shear modulus using the relation $G = E/2(1-\nu)$. However, Foo *et al* [36] state the existence of a significant anisotropy, with moduli E_1 = 3.40 GPa and E_2 = 2.46 GPa, with a difference between moduli of 38%. It should be noted that the testing performed by Foo *et al* appears to have been executed on unimpregnated Nomex paper. Most Nomex honeycombs are impregnated at least once with phenolic resin, and Hähnel et al [37] show that resin content qualitatively affects the behaviour of Nomex paper; dry paper behaves in a ductile manner, and each subsequent resin impregnation increases its stiffness and makes it behave in a more brittle manner. Hähnel et al [38] provide also comprehensive mechanical properties for resin-impregnated Nomex paper, and the values from the latter paper have been used in this work's normalisation.

Figure 11 to Figure 16 show the flatwise compression and shear properties of SILICOMB obtained in this work, compared to commercially available cores. All external honeycomb data was obtained from open literature datasheets [12], [39]–[41]. Figure 11 shows a comparison of the relative compressive modulus between the SILICOMB topology and several families of commercially available honeycombs. There is a strong sensitivity between density and modulus, despite the inclusion of the relative density as a factor in the normalisation, suggesting that the normalisation does not completely capture the effect of the parameters it is supposed to factor out. It can be observed that the flatwise compressive modulus of the SILICOMB is significantly lower than other honeycombs. However, it is important to note that the flatwise modulus of the SILICOMB topology was determined through unsupported (bare) compression tests (i.e. without face sheets), whereas the moduli of other honeycombs were determined through supported compression. This

inconsistency in the support conditions between tests results in qualitatively different behaviour of the honeycombs [42]–[45]. As a result, the observed stiffness is significantly reduced compared to supported honeycombs, and the magnitude of this effect dwarfs any effect of differences in cell geometry. Figure 12 and Figure 13 show the normalised results related to the 13 and 23 shear moduli respectively. Contrary to what one may expect, there appears to exist a nonlinear inverse relationship between density and the relative shear modulus. This is probably due to the normalisation process; the relative density is included in the same way as for the compressive results, but the way in which it affects shear and compressive modulus is different. For a given density the non-metallic honeycombs generally outperform the metallic ones, which suggests that the core material choice has a qualitative effect on honeycomb shear stiffness, as well as a quantitative effect (the latter should be taken into account by the use of the normalisation). The SILICOMB topology features a lower stiffness compared to the one belonging to commercial honeycombs. However – and differently from the flatwise compressive tests – all specimens are necessarily supported by plates acting as face skins to allow the shear testing to be performed. Non-metallic flex-core configurations seem to perform well at constant density. Figure 14 shows a comparison of relative compressive strength between the SILICOMB and the commercial honeycombs. There is significant separation between the different types of cellular solids, particularly between metallic and non-metallic cores. The Kirigami SILICOMB is placed between the two aforementioned groups. The separation between metallic and non-metallic cores could be due to the qualitative difference in failure mechanisms between metallic/non-metallic honeycombs [45]. However, in this case the normalisation is largely responsible; looking at the raw data, the results of the different honeycomb groups are very close together in terms of strength for a given density. When dividing by the elastic modulus to normalise, the aluminium honeycombs are divided by 70GPa, whereas the Nomex honeycombs are averaged by ~3GPa modulus.

Figure 15 and Figure 16 show the data related to the 13 and 23 shear strength respectively. It is again possible to identify a clear separation between the metallic and non-metallic honeycombs. The SILICOMB topology performs between the two groups; in the 23-direction its shear strength is very close to that of non-metallic cores with similar density.

4.1 Discussion

Figure 7, Figure 8, and Figure 9 show the analytical predictions compared to the mechanical test results. The analytical strength predictions show in general good agreement with the experimental results in the case of the flatwise compression. The position of the experimental results relative to the analytical predictions suggests that the actual boundary conditions are somewhere between those used in the analytical model. In

the case of the transverse shear the analytical model underestimates the strength for both shear directions. This could be due to the fact that the shear specimens are significantly more restrained than the compression ones because they are bonded to the loading platens. The stiffness of the Kirigami SILICOMB PEEK honeycombs is low compared to that of commercial counterparts (even in the case of supported testing), but its strength is comparable. This difference is probably largely due to the epoxy adhesive used in the joints during the manufacturing. As can be seen in Figure 3f, the epoxy forms fillets between neighbouring walls. These fillets have a number of effects, increasing first the relative density of the honeycomb, which is directly linked to the flatwise modulus [1]. Secondly, they restrain rotations within the joints, thus confining the in-plane deformation mechanisms. In terms of strength, the epoxy has two effects. Firstly, it changes the boundary conditions of the wall edges where they meet at the joints, and secondly it contributes to modify the effective aspect ratio of each cell wall. Both of these effects will change the buckling behaviour compared to SILICOMB without epoxy inserts. Simone and Gibson [46] show that fillets at the joints can increase both the modulus and strength of cellular structures, even if the material for the fillet is taken from the mid-span of the cell walls, at the expense of cell wall thickness. In the case of SILICOMB, the wall thickness is unaffected and material is simply added to the joints, so the effect is likely to be even more pronounced. Finally, it is likely that the Poisson's ratio of SILICOMB will also be affected. SILICOMB achieves its zero-ν behaviour through the rotation and bending of joints as an in-plane deformation mechanism [47]. Because the epoxy restrains the joints, it is likely that some coupling occurs locally, resulting in a non-zero Poisson's ratio global effect. When no further material phase is present in the joints, the global Poisson's ratio is zero [22]. An indirect effect of the ventilation holes is to create a stress concentration, where failure could potentially initiate. In compression, SILICOMB cell walls were observed to buckle, after which material failure occurred during the crushing phase. Because of the small size of the ventilation holes relative to the cell wall width, their effect on the buckling load will have been very small [48]. It is possible that the ventilation holes affected the crushing mechanism. In shear, the ventilation holes will again have little effect on the buckling load due to their small size [49], [50]. However, in this case they significantly affect post-buckling failure; a plate undergoing shear buckling carries most of the load along the tension diagonal [51], and because the presence of the holes increases the local tensile stress [49] they provide a crack initiation point. It can be seen from Figure 10 that diagonal cracks have formed at the holes, lowering the shear strength of the SILICOMB topology. It is also interesting to note the shape of the buckles; the two adjacent *l*-walls in each cell have buckled as one, with the diagonal buckles going from the top left corner of the left cell wall to the bottom right corner of the right cell wall. This suggests that the stiffening effect of the fold between cell walls is less than the stiffening effect of the joints where cell walls intersect.

The relative cell size to other dimensions of the honeycomb is an important parameter of the honeycomb configuration, along with relative density and sheet material properties [36], [52], [53]. Considering the cell size relative to the specimen size, Foo et al [36] show that the out-of-plane modulus depends strongly on the number of cells present in the sample, and Onck et al [52] analyse the effect of the specimen size relative to cell size on a variety of honeycomb characteristics. They show that when the specimen size is comparable to the cell size, the specimen properties are significantly different from the bulk properties predicted for an infinite honeycomb. However, as the specimen size is increased to many times the cell size, the specimen properties approach the bulk properties. Onck and co-workers conclude that this effect is largely due to the proportion of the specimen material present in the open cell walls around the edge of the specimen, which contribute little to the modulus or strength of the honeycomb. The border of open cells around a specimen is made up of truncated closed cells, and as such it must be less than one cell size in width, regardless of specimen size. However the inner portion of the specimen which is made up of closed cells is proportional to the square of specimen size, so as the specimen size becomes bigger the closed cell properties dominate and the effect of the open cells becomes less significant. Onck et al [52] applied this principle to analyse in-plane compression and shear of honeycombs, but the same principle also applies in the cases of out-of-plane compression and shear; In flatwise compression the cell walls can be considered as plates in buckling with clamped edges and free ends [33]. In this case an open cell wall has one free edge, which significantly lowers its buckling load compared to a closed cell with edges clamped. In shear the honeycomb carries the load through shear flow in the cell walls [33]. An open cell wall has again different boundary conditions for buckling, and it also does not form a closed circuit through which to transmit shear flow. One can therefore argue that the open cell walls contribute very little to the out-of-plane stiffness and strength, and their presence should affect the specimen performance in a way similar to that predicted by Onck et al [52]. The minimum specimen size required to render size effects insignificant depends on the type of loading and fixity conditions, amongst other things. Onck [53] reports also that size effects vanish for specimens larger than 2 and 7 cell sizes for in-plane shear and compression, respectively. He attributes the difference to the fact that shear specimens have strong edge boundary conditions (BC) (open cell wall edges fixed to loading platens) and compression specimens have instead weak edge BCs (open cell walls free). The sizes of the SILICOMB specimens in terms of cell size are given in Table 1. The minimum specimen dimension in multiples of cell size is 3, for the type B shear specimens. It is also important to consider cell size relative to honeycomb thickness; this affects cell wall buckling, which is the dominant failure mode of SILICOMB. If we consider the cell walls as plates undergoing Eulerian buckling, as in Gibson and Ashby [1], then the buckling strength of the cell walls is determined in part by their aspect ratio. The aspect ratio is dependent on the cell size and the honeycomb thickness. Neither of these parameters is taken into account by the normalisation. Lira et al

[20] analysed the SILICOMB geometry in transverse shear, and their results indicate that increasing "gauge thickness ratio" (honeycomb thickness/cell wall length) – hence increasing the cell aspect ratio – results in a decrease in shear moduli. Paik et al [43] observe from experiments that increasing the thickness of the honeycomb core relative to the cell size can delay the onset of plastic deformation and hence affect the compressive strength of a sandwich panel. Figure 17 shows that the SILICOMB specimens have a significantly higher cell size than any of the commercial honeycombs to which they are compared (more than double, in most cases). However, the thickness of the SILICOMB specimens is only slightly larger than that of the commercial cores (15mm vs 12.5mm; a factor of 1.2). It is possible that this affected the comparison of honeycomb strengths.

5 Conclusions

The work has shown the feasibility of manufacturing the ZPR SILICOMB geometry with PEEK core material using current thermoforming technology. The advantages of the thermoforming technique coupled to the Kirigami process are the reduced processing cost compared to an autoclave, and faster processing times than thermoset composites due to lack of a cure cycle. Disadvantages of the current manufacturing layout are the high amount of manual labour involved, and the difficulty of producing uniform joints and using large amounts of adhesives. The drawbacks of the current production process can be overcome by moving towards press-forming techniques, which allow faster processing and the use of male/female moulds to achieve better forming accuracy than the male mould/vacuum bag used in thermoforming. It is possible to laser weld PEEK film [54], providing therefore another solution to replace the current adhesive joints. The transverse properties of SILICOMB have been investigated experimentally, and compared to the properties of commercially available honeycombs. Several factors have been identified which have affected the SILICOMB testing, the most important of which is the effect of the epoxy inserts.

6 Acknowledgements

This work was performed under the European Commission project NMP4-LA-2010-246067 (M-RECT (http://cordis.europa.eu/projects/rcn/94838_en.html)). The financial support from the European Commission is gratefully acknowledged. Special thanks go also to Mr Ian Chorley (ACCIS Technician) for the support during the manufacturing and testing of the PEEK honeycombs. The Authors are also grateful to Dr Alan Wood from Victrex plc (M-RECT Coordinator) for the advice provided about the processing of the PEEK films.

7 References

[1] L. J. Gibson and M. F. Ashby, *Cellular solids - Structure and properties*, 2nd ed. Cambridge University Press, 1997.

[2] F. Scarpa and P. J. Tomlin, "On the transverse shear modulus of negative Poisson's ratio honeycomb structures," *Fatigue Fract. Eng. Mater. Struct.*, vol. 23, no. 8, pp. 717–720, Aug. 2000.

[3] T. Lim, "Functionally graded beam for attaining Poisson-curving," *J. Mater. Sci. Lett.*, vol. 21, no. 24, pp. 1899–1901, 2002.

[4] A. Bezazi, F. Scarpa, and C. Remillat, "A novel centresymmetric honeycomb composite structure," *Compos. Struct.*, vol. 71, no. 3–4, pp. 356–364, Dec. 2005.

[5] J. N. Grima, R. Gatt, A. Alderson, and K. E. Evans, "On the potential of connected stars as auxetic systems," *Mol. Simul.*, vol. 31, no. 13, pp. 925–935, Nov. 2005.

[6] D. Prall and R. S. R. S. Lakes, "Properties of a chiral honeycomb with a poisson's ratio of — 1," *Int. J. Mech. Sci.*, vol. 39, no. 3, pp. 305–314, Mar. 1997.

[7] W. Miller, C. W. Smith, F. Scarpa, and K. E. Evans, "Flatwise buckling optimization of hexachiral and tetrachiral honeycombs," *Compos. Sci. Technol.*, vol. 70, no. 7, pp. 1049–1056, Jul. 2010.

[8] a. Lorato, P. Innocenti, F. Scarpa, A. Alderson, K. L. Alderson, K. M. Zied, N. Ravirala, W. Miller, C. W. Smith, and K. E. Evans, "The transverse elastic properties of chiral honeycombs," *Compos. Sci. Technol.*, vol. 70, no. 7, pp. 1057–1063, Jul. 2010.

[9] K. E. Evans, M. A. Nkansah, I. J. Hutchinson, and S. C. Rogers, "Molecular network design," *Nature*, vol. 353, no. 6340, pp. 124–124, Sep. 1991.

[10] J. N. Grima, L. Oliveri, D. Attard, B. Ellul, R. Gatt, G. Cicala, and G. Recca, "Hexagonal Honeycombs with Zero Poisson's Ratios and Enhanced Stiffness," *Adv. Eng. Mater.*, vol. 12, no. 9, pp. 855–862, Sep. 2010.

[11] K. Evans, "The design of doubly curved sandwich panels with honeycomb cores," *Compos. Struct.*, vol. 17, no. 2, pp. 95–111, Jan. 1991.

[12] Hexcel, “HexWeb® Aluminum Flex-Core® datasheet (accessed 2013-03-12).” .

[13] K. R. Olympio and F. Gandhi, “Zero Poisson’s Ratio Cellular Honeycombs for Flex Skins Undergoing One-Dimensional Morphing,” *J. Intell. Mater. Syst. Struct.*, vol. 21, no. 17, pp. 1737–1753, Dec. 2009.

[14] G. C. Engelmayr, M. Cheng, C. J. Bettinger, J. T. Borenstein, R. Langer, and L. E. Freed, “Accordion-like honeycombs for tissue engineering of cardiac anisotropy.,” *Nat. Mater.*, vol. 7, no. 12, pp. 1003–10, Dec. 2008.

[15] T. Bitzer, *Honeycomb technology - materials, design, manufacturing, applications and testing*, 1st ed. London: Chapman & Hall, 1997.

[16] J. N. Grima and D. Attard, “Molecular networks with a near zero Poisson’s ratio,” *Phys. Status Solidi*, vol. 248, no. 1, pp. 111–116, Jan. 2011.

[17] K. Olympio and F. Gandhi, “Zero-ν cellular honeycomb flexible skins for one-dimensional wing morphing,” in *48th Structures, Structural Dynamics, and Materials Conference, AIAA/ASME/ASCE/AHS/ASC, Honolulu, Hi. April*, 2007, no. April, pp. 23–26.

[18] H. Kimizuka, H. Kaburaki, and Y. Kogure, “Mechanism for negative poisson ratios over the alpha-beta transition of cristobalite, SiO2: A molecular-dynamics study,” *Phys. Rev. Lett.*, vol. 84, no. 24, pp. 5548–51, Jun. 2000.

[19] J. N. Grima, E. Manicaro, and D. Attard, “Auxetic behaviour from connected different-sized squares and rectangles,” *Proc. R. Soc. A Math. Phys. Eng. Sci.*, vol. 467, no. 2126, pp. 439–458, Aug. 2010.

[20] C. Lira, F. Scarpa, Y. H. Tai, and J. R. Yates, “Transverse shear modulus of SILICOMB cellular structures,” *Compos. Sci. Technol.*, vol. 71, no. 9, pp. 1236–1241, Jun. 2011.

[21] Y. Chen, F. Scarpa, C. Remillat, I. Farrow, Y. Liu, and J. Leng, “Curved Kirigami SILICOMB cellular structures with zero Poisson’s ratio for large deformations and morphing,” *J. Intell. Mater. Syst. Struct.*, vol. 0, no. 0, pp. 1–13, Sep. 2013.

[22] K. Virk, a Monti, T. Trehard, M. Marsh, K. Hazra, K. Boba, C. D. L. Remillat, F. Scarpa, and I. R. Farrow, “SILICOMB PEEK Kirigami cellular structures: mechanical response and energy dissipation through zero and negative stiffness,” *Smart Mater. Struct.*, vol. 22, no. 8, p. 084014, Aug. 2013.

[23] T. Nojima and K. Saito, “Development of Newly Designed Ultra-Light Core Structures,” *JSME Int. J. Ser. A*, vol. 49, no. 1, pp. 38–42, 2006.

[24] T. Nojima, “Origami Modeling of Functional Structures based on Organic Patterns,” in *Presentation Manuscript at VIPSI Tokyo*, 1996.

[25] K. Saito, F. Agnese, and F. Scarpa, “A Cellular Kirigami Morphing Wingbox Concept,” *J. Intell. Mater. Syst. Struct.*, vol. 22, no. 9, pp. 935–944, Aug. 2011.

[26] K. Saito, S. Pellegrino, and T. Nojima, “Manufacture of Arbitrary Cross-Section Composite Honeycomb Cores Based on Origami Techniques,” in *Proceedings of the ASME 2013 International Design Engineering Technical Conferences and Computers and Information in Engineering Conference*, 2013.

[27] Y. Hou, R. Neville, F. Scarpa, C. Remillat, B. Gu, and M. Ruzzene, “Graded conventional-auxetic Kirigami sandwich structures: flatwise compression and edgewise loading,” *Compos. Part B Eng.*, Nov. 2013.

[28] D. D. Howell, A. M. Lizotte, and D. L. Dequine, “Design, Analysis, Manufacture and Test of a continuous fiber reinforced thermoplastic stringer with local reinforcements,” in *SAMPE 2013 proceedings - education & green sky - Materials technology for a better world*, 2013.

[29] M. Lauzon, “Diversified Plastics Inc., PEEK playing role in space probe,” *Plastics News*, 2012. [Online]. Available: http://www.plasticsnews.com/article/20120504/NEWS/305049956. [Accessed: 06-Jan-2014].

[30] Victrex PLC, “APTIV Film Thermoforming Guide,” 2011.

[31] ASTM International, “C365 / C365M Test Method for Flatwise Compressive Properties of Sandwich Cores,” 2011.

[32] ASTM International, “C273 / C273M Test Method for Shear Properties of Sandwich Core Materials,” 2011.

[33] J. Zhang and M. F. Ashby, “The out-of-plane properties of honeycombs,” *Int. J. Mech. Sci.*, vol. 34, no. 6, pp. 475–489, Jun. 1992.

[34] W. C. Young and R. G. Budnyas, *Roark's Formulas for Stress and Strain*, 7th ed. McGraw-Hill, 2002.

[35] DuPont, "NOMEX® Type 410 Technical Data Sheet (accessed 2013-03-15)." .

[36] C. C. Foo, G. B. Chai, and L. K. Seah, "Mechanical properties of Nomex material and Nomex honeycomb structure," *Compos. Struct.*, vol. 80, no. 4, pp. 588–594, Oct. 2007.

[37] F. Hähnel and K. Wolf, "Evaluation of the material properties of resin-impregnated Nomex® paper as basis for the simulation of the impact behaviour of honeycomb sandwich," in *Proceedings of the 3rd international conference on composites testing and model identification*, 2006, pp. 1–2.

[38] F. Hähnel, K. Wolf, A. Hauffe, K. a. Alekseev, and I. M. Zakirov, "Wedge-shaped folded sandwich cores for aircraft applications: from design and manufacturing process to experimental structure validation," *CEAS Aeronaut. J.*, vol. 2, no. 1–4, pp. 203–212, Aug. 2011.

[39] Hexcel, "HexWeb® Nonmetallic Flex-Core® datasheet (accessed 2013-03-12)." .

[40] Hexcel, "HexWeb® HRH-10 datasheet (accessed 2013-03-12)." .

[41] Hexcel, "HexWeb® HRH-78 datasheet (accessed 2013-03-12)." .

[42] J. F. Davalos, "Buckling Behavior of Honeycomb FRP Core with Partially Restrained Loaded Edges under Out-of-plane Compression," *J. Compos. Mater.*, vol. 39, no. 16, pp. 1465–1485, Aug. 2005.

[43] J. Kee Paik, A. K. Thayamballi, and G. Sung Kim, "The strength characteristics of aluminum honeycomb sandwich panels," *Thin-Walled Struct.*, vol. 35, no. 3, pp. 205–231, Nov. 1999.

[44] a. R. Othman and D. C. Barton, "Failure initiation and propagation characteristics of honeycomb sandwich composites," *Compos. Struct.*, vol. 85, no. 2, pp. 126–138, Sep. 2008.

[45] Y. Aminanda, B. Castanié, J.-J. Barrau, and P. Thevenet, "Experimental Analysis and Modeling of the Crushing of Honeycomb Cores," *Appl. Compos. Mater.*, vol. 12, no. 3–4, pp. 213–227, May 2005.

[46] A. E. Simone and L. J. Gibson, "Effects of solid distribution on the stiffness and strength of metallic foams," *Acta Mater.*, vol. 46, no. 6, pp. 2139–2150, 1998.

[47] C. Lira, F. Scarpa, M. Olszewska, and M. Celuch, "The SILICOMB cellular structure: Mechanical and dielectric properties," *Phys. Status Solidi*, vol. 246, no. 9, pp. 2055–2062, Sep. 2009.

[48] D. J. Vandenbrink and M. P. Kamat, "Post-buckling response of isotropic and laminated composite square plates with circular holes," *Finite Elem. Anal. Des.*, vol. 3, no. 3, pp. 165–174, Oct. 1987.

[49] ESDU, "75034 INITIAL BUCKLING STRESS, MAXIMUM DIRECT STRESS AND SHEAR STRAIN OF SQUARE PLATES IN SHEAR WITH CENTRAL CIRCULAR HOLES," 1975.

[50] N. E. Shanmugam, "Openings in Thin-Walled steel structures," *Thin-Walled Struct.*, vol. 28, no. 3–4, pp. 355–372, Jul. 1997.

[51] ESDU, "02005 Flat panels in shear – post-buckling analysis," 2002.

[52] P. Onck, E. Andrews, and L. Gibson, "Size effects in ductile cellular solids. Part I: modeling," *Int. J. Mech. Sci.*, vol. 43, pp. 681–699, 2001.

[53] P. Onck, "Scale effects in cellular metals," *MRS Bull.*, no. April, pp. 279–283, 2003.

[54] N. Amanat, C. Chaminade, J. Grace, D. R. McKenzie, and N. L. James, "Transmission laser welding of amorphous and semi-crystalline poly-ether–ether–ketone for applications in the medical device industry," *Mater. Des.*, vol. 31, no. 10, pp. 4823–4830, Dec. 2010.

[55] Granta, "CES EduPack material selector software." 2012.

8 Figures

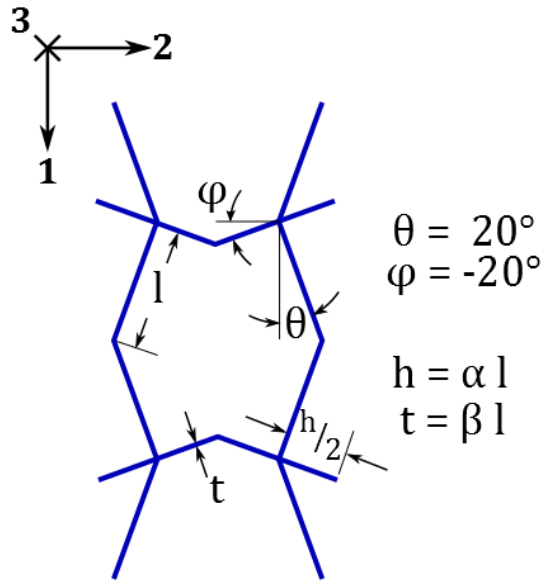

Figure 1: The SILICOMB unit cell (redrawn from [20])

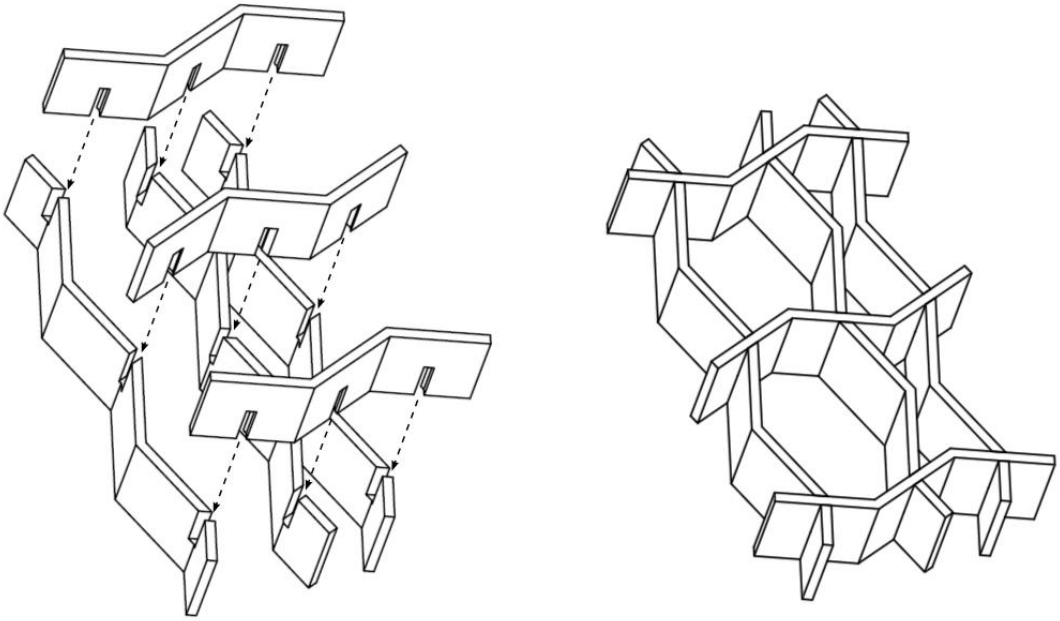

Figure 2: Interlocking strips form SILICOMB geometry.

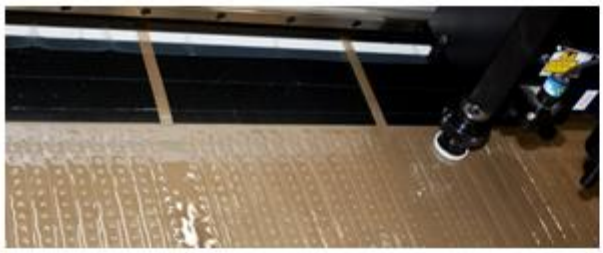

a) Cutting PEEK strips using Blackman & White Genesis cutter

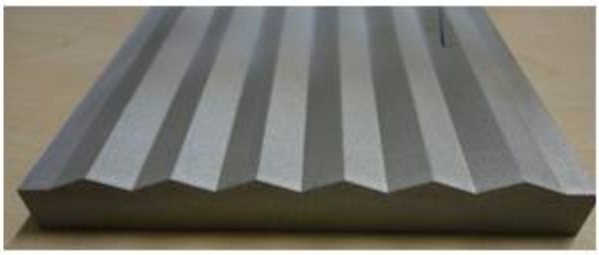

b) Corrugated mould

c) Strips are fixed before forming to maximise fold accuracy

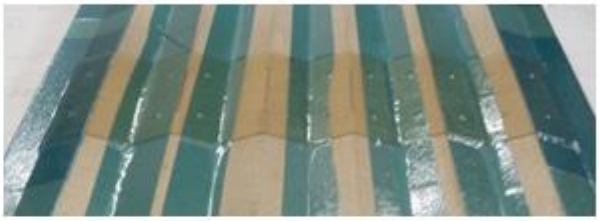

d) Strips after forming in Formech FM1 vacuum forming table

e) The slots on strips are interlocked

f) Epoxy adhesive is applied to fix joints

g) Epoxy is cured at 70°C for 1 hour with weights to keep the sample flat

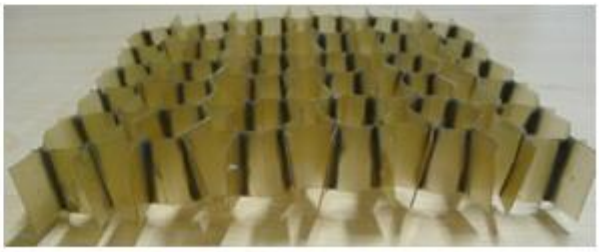

h) Finished (compression) sample

Figure 3: SILICOMB manufacturing process

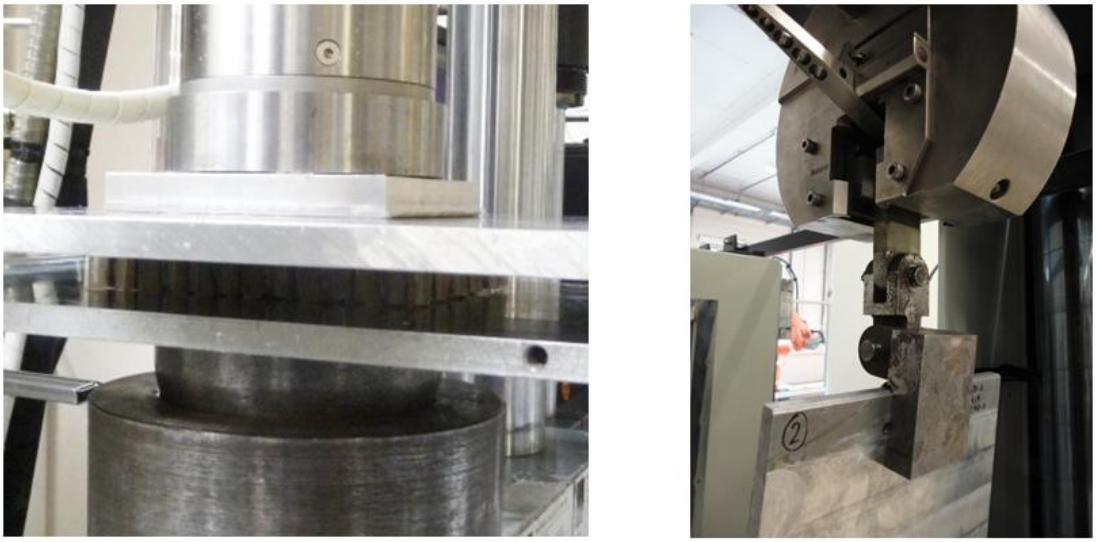

Figure 4: Self-aligning test fixtures for a) flatwise compression and b) single-lap shear

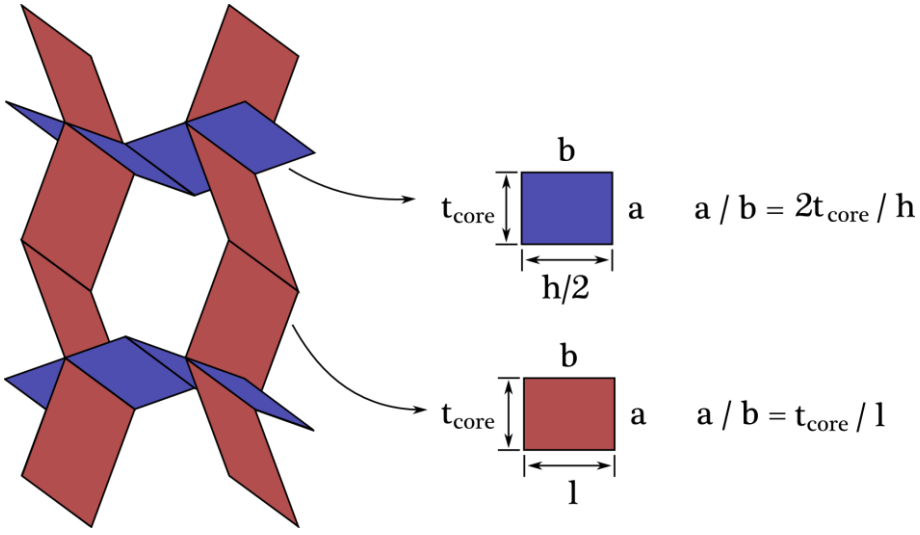

Figure 5: SILICOMB unit cell broken down into l-walls and h-walls.

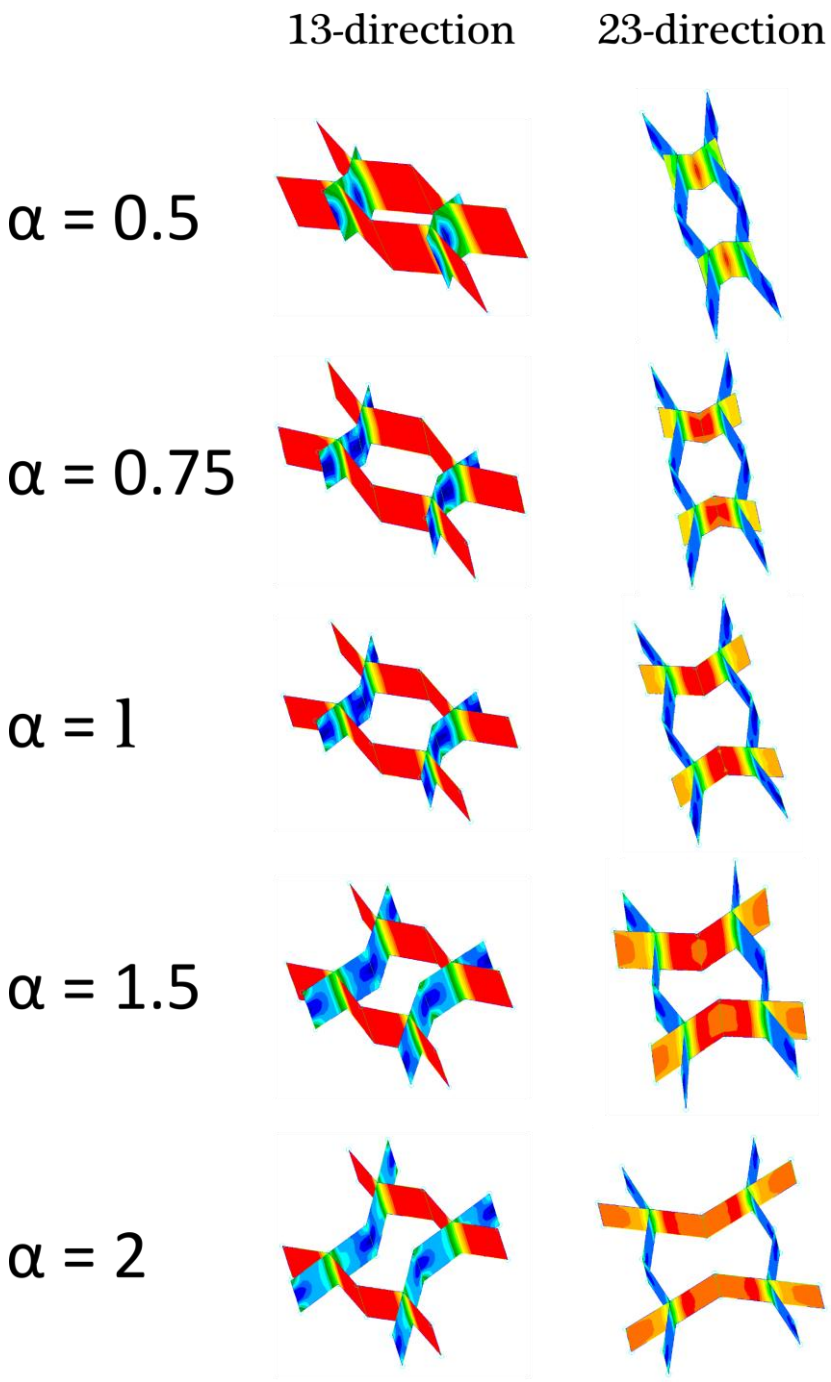

Figure 6: Von Mises stress distribution for a range of α values as predicted by finite element analysis. α was varied by holding l constant and varying h.

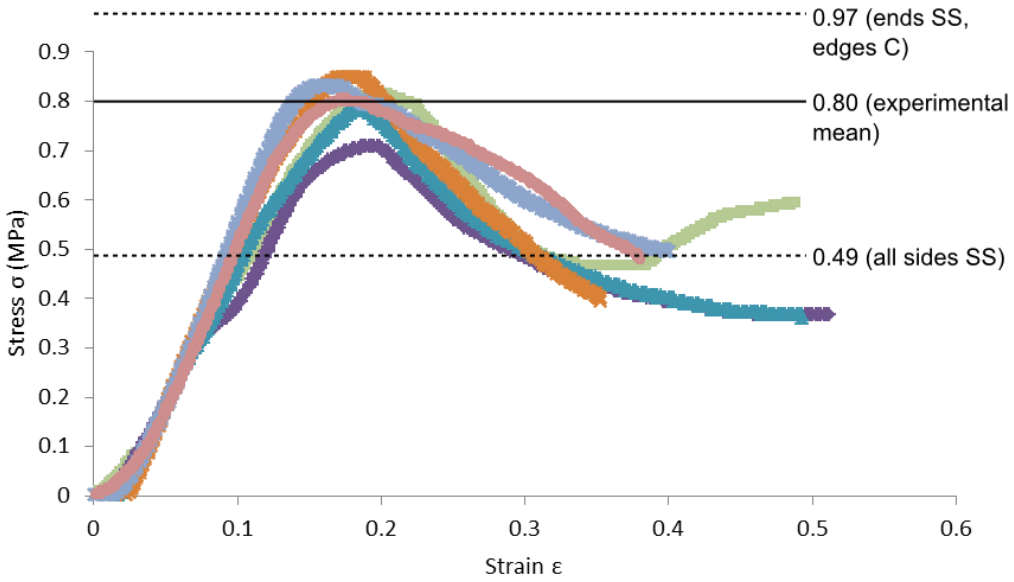

Figure 7: Compression test stress-strain curves with analytical predictions.

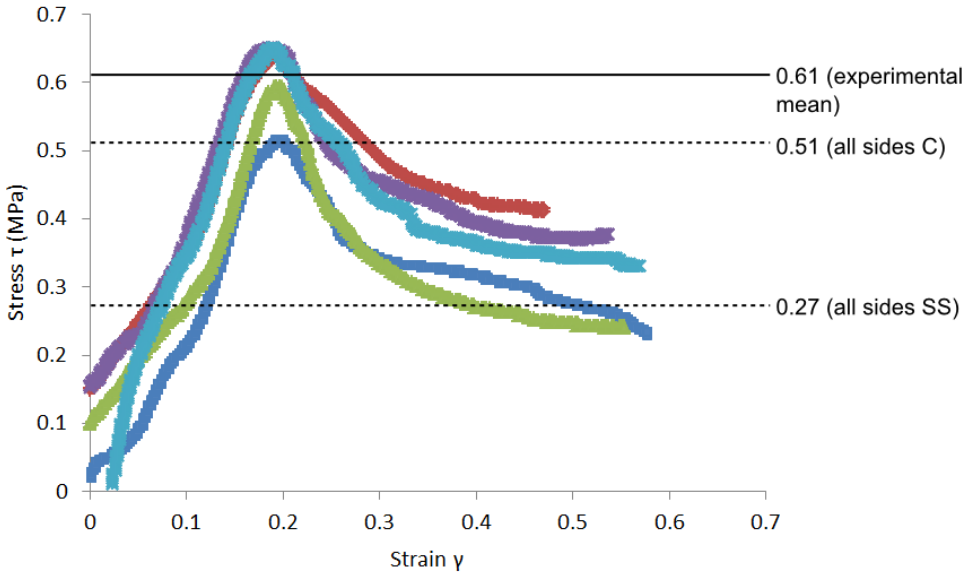

Figure 8: Shear stress-strain curves for category A (13-shear) with analytical predictions.

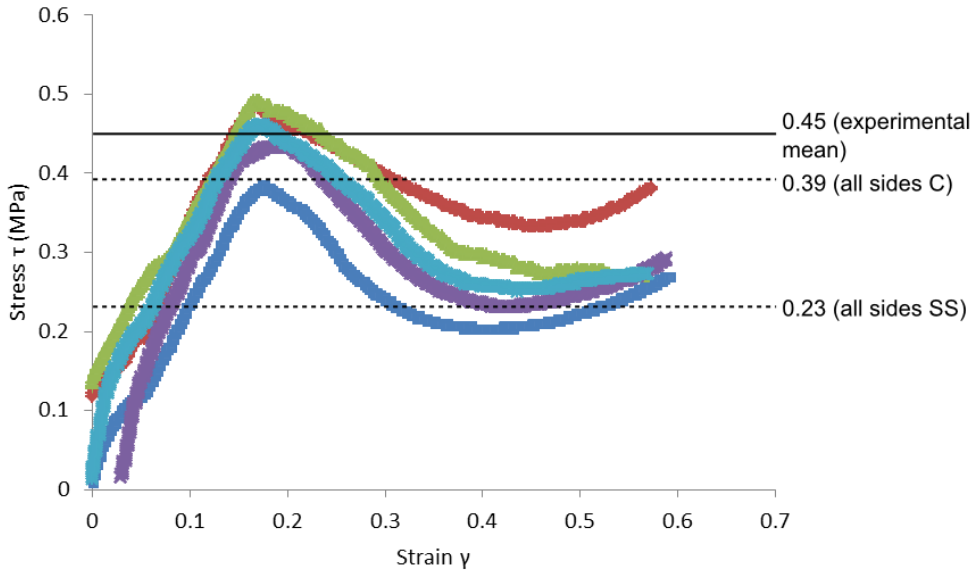

Figure 9: Shear stress-strain curves for category B sample (23-shear) with analytical predictions.

Figure 10: Tearing of the ventilation holes in A-type shear samples

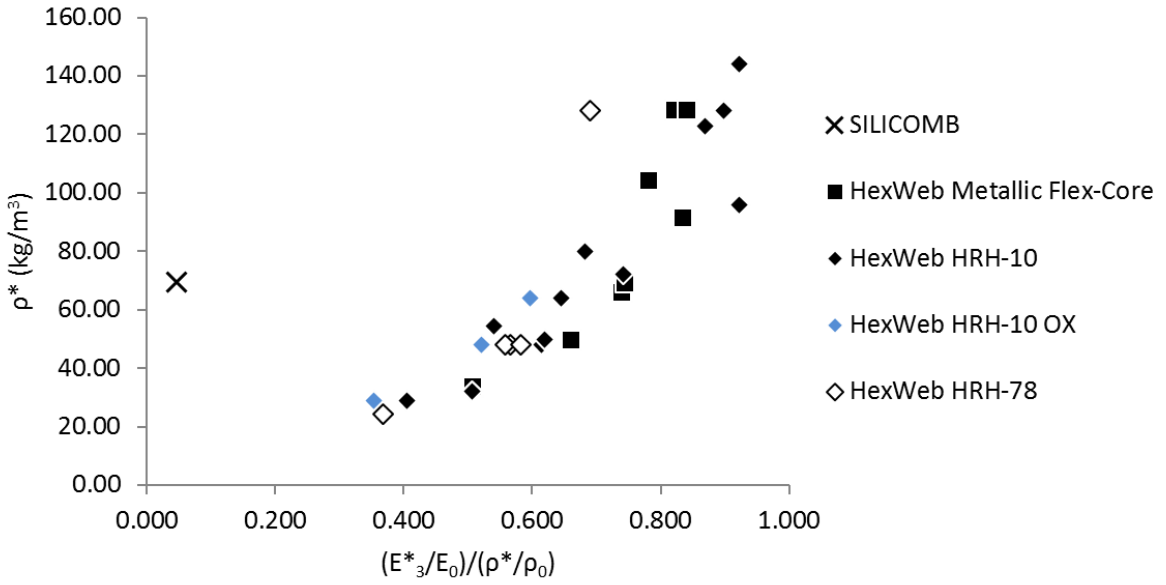

Figure 11: Flatwise compressive modulus of SILICOMB compared to commercially available honeycombs. Note that in this case the SILICOMB was tested in unsupported compression, whereas the commercially available cores were tested under supported boundary conditions.

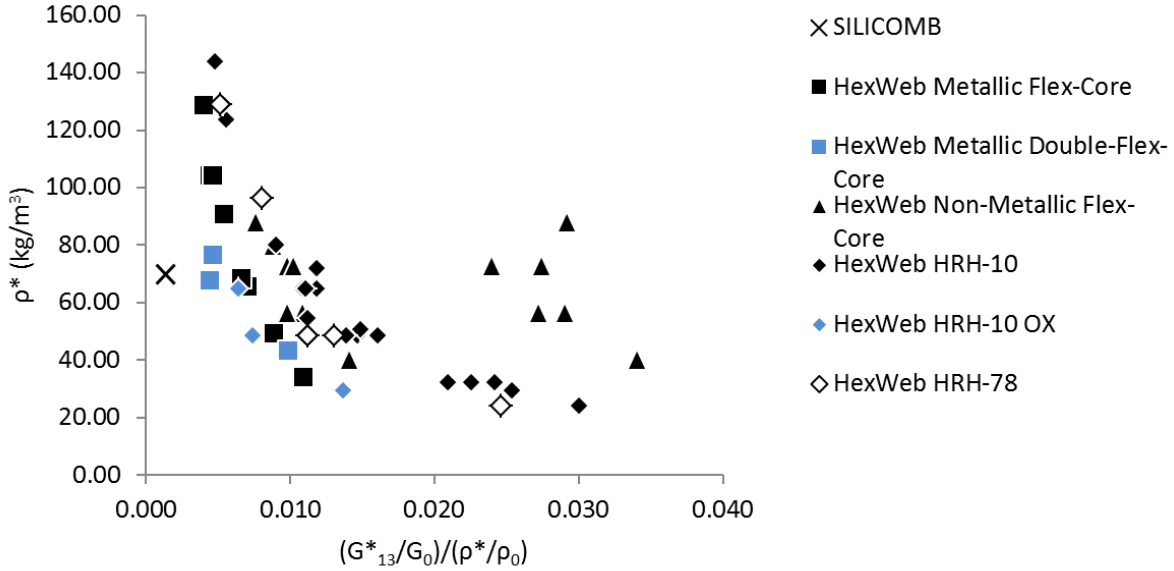

Figure 12: 13-direction shear moduli of SILICOMB compared to commercially available honeycombs.

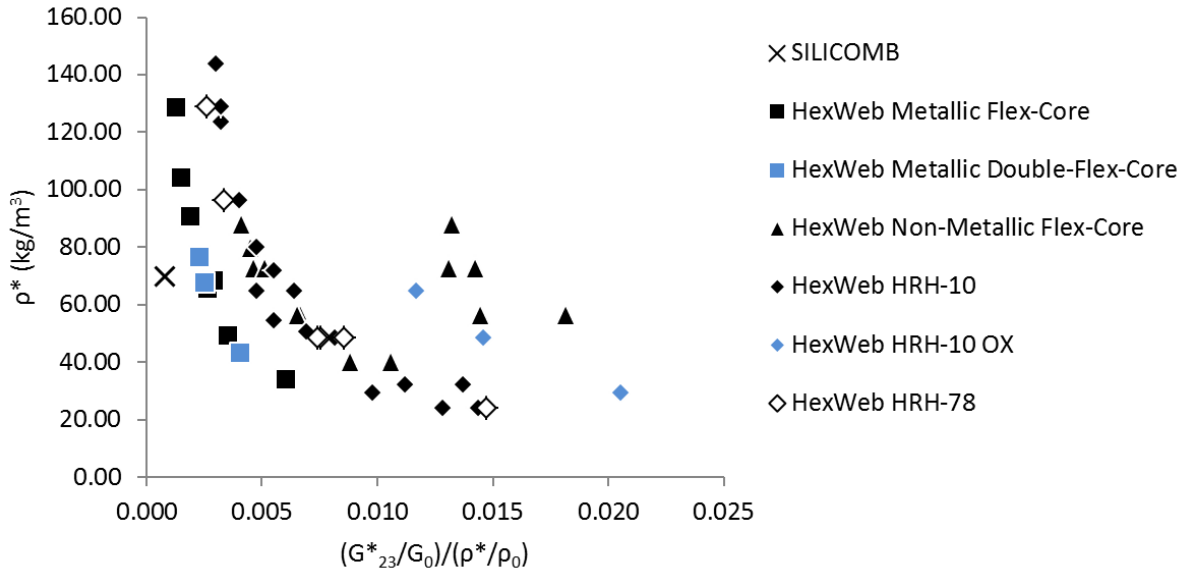

Figure 13: 23-direction shear moduli of SILICOMB compared to commercially available honeycombs.

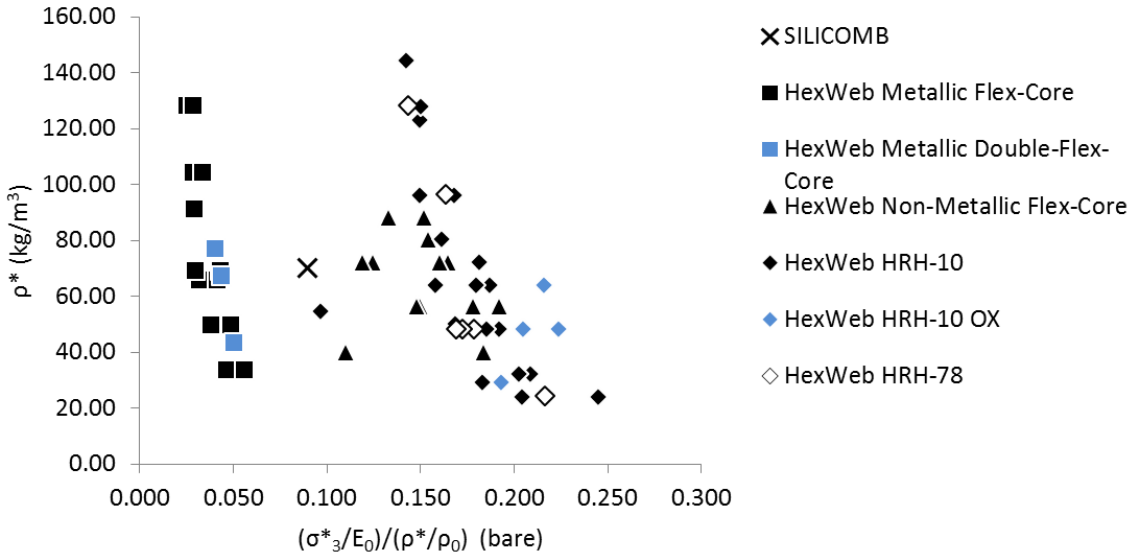

Figure 14: Flatwise ultimate compressive strength of SILICOMB compared to commercially available honeycombs.

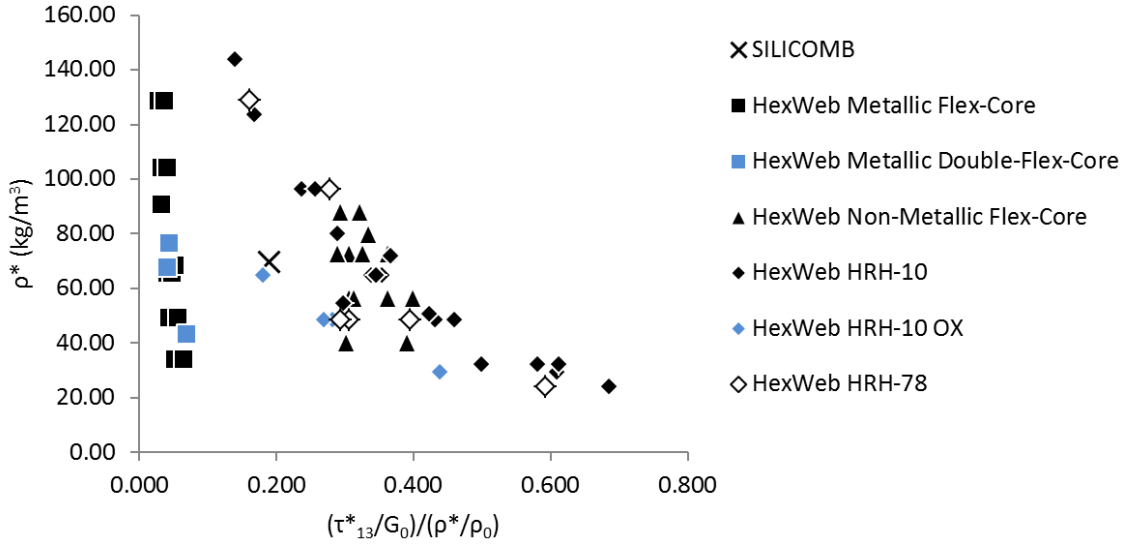

Figure 15: 13-direction ultimate shear strengths of SILICOMB compared to commercially available honeycombs.

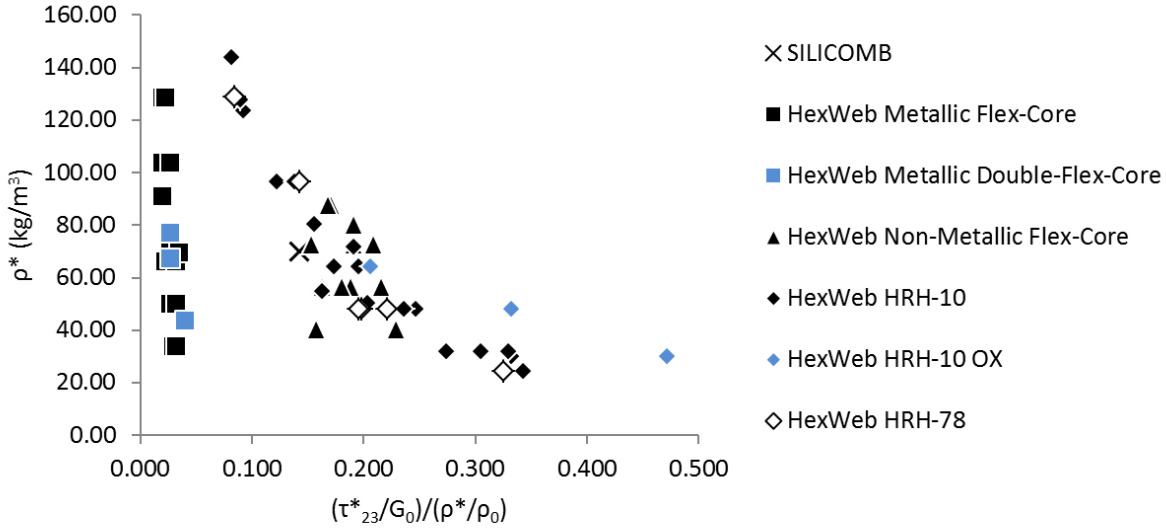

Figure 16: 23-direction ultimate shear strengths of SILICOMB compared to commercially available honeycombs.

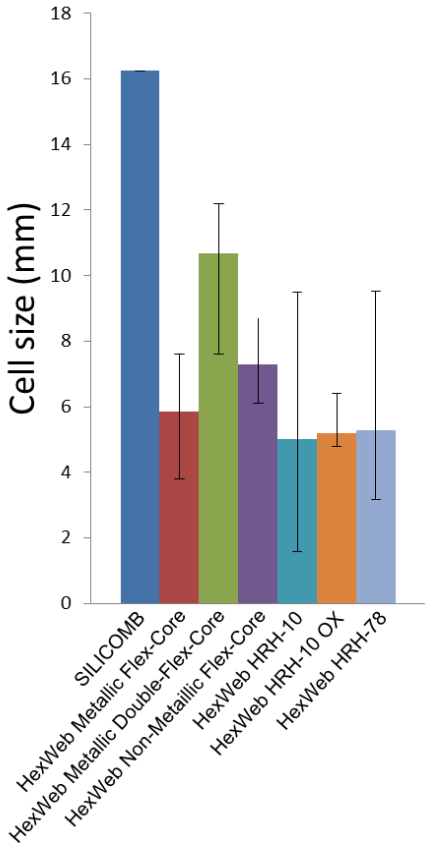

Figure 17: Cell size (measured in W-direction). The error bars represent the spread of cell size over each "family" of honeycombs.

9 Tables

Table 1: SILICOMB specimen properties

		Comp	Shear A (13 shear)	Shear B (23 shear)	
Number of cells (1-dir'n)	n_{c1}	5	9	3	-
Number of cells (2-dir'n)	n_{c2}	11	5	19	-
Length (1-dir'n)	L	112.8	187.9	56.4	mm
Width (2-dir'n)	W	112.8	56.4	187.9	mm
Specimen thickness	t_{core}	15	15	15	mm
Material thickness	t	0.25	0.25	0.25	mm
Horizontal rib length	h	10	10	10	mm
Vertical rib length	l	10	10	10	mm
Aspect ratio (h/l)	α	1	1	1	-
Thickness ratio (t/l)	β	0.025	0.025	0.025	-
Theta	θ	20	20	20	degrees
Phi	φ	-20	-20	-20	degrees

Relative density	ρ^*/ρ_0	0.055	0.055	0.055	-

Table 2: Cell wall buckling coefficients. Coefficients from Roark's formulas for Stress and Strain [34]. Letter denotes loading type (K = compression; C = shear). Subscript denotes cell wall type (l or h). Superscript denotes BCs (SS = simply supported; C = clamped).

Coeff.	Coeff. Value	*a* (mm)	*b* (mm)	*a/b*	Edge BCs	End BCs
K_l^{SS}	3.57	15	10	1.5	SS	SS
$K_l^{SS/C}$	7.20	15	10	1.5	C	SS
K_h^{SS}	3.29	15	5	3	SS	SS
$K_h^{SS/C}$	6.40	15	5	3	C	SS
C_l^{SS}	5.84	15	10	1.5	SS	SS
C_l^{C}	11.10	15	10	1.5	C	C
C_h^{SS}	5.02	15	5	3	SS	SS
C_h^{C}	8.44	15	5	3	C	C

Table 3: Mechanical properties of honeycomb constituent materials.

Honeycomb	Constituent material	E_0 (GPa)	v	G (GPa)	ρ (kg/m^3)	Source
SILICOMB	Victrex Aptiv 2000-250 PEEK film	2.3	0.4	0.82	1260	Mechanical testing at Bristol
HexWeb Metallic Flex-Core	Al 5052/5056 alloy foil	70	0.33	27	2670	Ref. [55]
HexWeb Metallic Double Flex-Core						
HexWeb Non-metallic Flex-Core	Aramid fibre/paper sheets + phenolic resin	3.4	0.4	1.21	1100	Ref. [38]
HexWeb HRH-10						
HexWeb HRH-78						